New Journal of Physics
The open access journal at the forefront of physics

Deutsche Physikalische Gesellschaft DPG
IOP Institute of Physics

Published in partnership with: Deutsche Physikalische Gesellschaft and the Institute of Physics

OPEN ACCESS

RECEIVED
5 December 2014

REVISED
6 February 2015

ACCEPTED FOR PUBLICATION
13 February 2015

PUBLISHED
27 March 2015

PAPER

Large morphological sensitivity of the magneto-thermopower in Co/Cu multilayered systems

Voicu Popescu and Peter Kratzer

Faculty of Physics and Center for Nanointegration (CENIDE), University of Duisburg-Essen, Lotharstraße 1, 47057 Duisburg, Germany

E-mail: voicu.popescu@uni-due.de

Keywords: thermomagnetic effects, magnetotransport effects, Co/Cu multilayers, first principles calculations

Abstract

We present results of first-principles calculations on the transport properties, both under an electric field or a temperature gradient, in Co/Cu multilayered systems. The various effects brought about by the changes in the morphological parameters, such as the number of repeats and the layer thickness, are discussed in a systematic way. Our calculations show that the Seebeck coefficient and the magneto-thermopower (MTP) converge rather rapidly with the number of Co repeats. In the range of thin Co layers, we find strong variations in the amplitude and sign of both the Seebeck coefficient and the MTP. These large variations, which have no correspondent in the (magneto)conductance, are shown to be the result of quantum well states present in the minority spin channel of thin Co layers.

1. Introduction

Metallic heterostructures of alternating magnetic and non-magnetic materials have been in the focus of research for more than two decades. These intense experimental and theoretical investigations have been triggered by the giant magnetoresistance (GMR) effect [1]. Currently the keystone of standard magnetic field sensors, the GMR denotes the large change in resistance caused by the switching from an anti-parallel to a parallel magnetic alignment of the adjacent magnetic layers under an external magnetic field. An analogous phenomenon could be observed in multilayered structures subject to a temperature gradient, in which case the central quantity measuring the magnetic response was the magneto-thermopower (MTP). These experiments, performed both in the current-in-plane (CIP) [2–5] as well as in the current-perpendicular-to-the-plane (CPP) geometry [6], mark the first successful attempts of linking the heat flow with the spin degree of freedom, paving the way towards the emerging field of spin calorics [7].

In recent years, the ability to fabricate multilayer samples in the form of nanopillars has opened up the possibility to detect their internal state of magnetization. The small diameter of the pillars, which results in small thermal conductance, in conjunction with a strong heating by pulsed laser illumination of the pillar top allows one to build up sizable temperature gradients [8–12], causing a thermoelectric voltage whose magnitude and sign reflects the internal magnetization state. This method of detection, depicted schematically in figure 1(a), may be even more sensitive than the CPP-GMR effect. Indeed, the magnetic response of a GMR device is usually quantified through the GMR ratio, expressing the relative difference of the resistances of the heterostructure in the two magnetic alignments, parallel (P) and anti-parallel (AP). Equivalently, one can use the conductance g as defining quantity to express the magneto-conductance (MC) ratio as:

$$\mathrm{MC}(\%) = \frac{g_\mathrm{P} - g_\mathrm{AP}}{g_\mathrm{P}} \times 100. \tag{1}$$

The MTP ratio can be introduced quite analogously:

$$\mathrm{MTP}(T)(\%) = \frac{S_\mathrm{P}(T) - S_\mathrm{AP}(T)}{S_\mathrm{AP}(T)} \times 100, \tag{2}$$

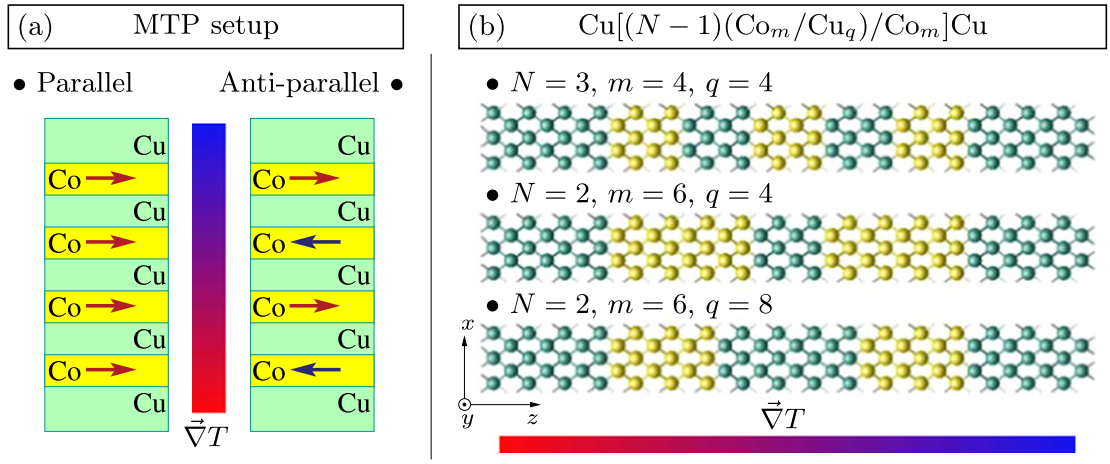

Figure 1. Schematic representations of (a) the generic setup of a multilayered Co/Cu system providing an MTP signal; and (b) selected structural models of the $\mathrm{Cu}[(N-1)(\mathrm{Co}_m/\mathrm{Cu}_q)/\mathrm{Co}_m]\mathrm{Cu}$ systems investigated in this work, illustrating the meaning of the various geometrical parameters N, m, and q. N is the number of Co repeats embedded in Cu, while m and q represent the thickness in atomic monolayers (MLs) of the Co (yellow) and Cu (dark green) layers. The figure only shows the scattering region, with the half-infinite Cu leads extending left and right along the z direction. The whole system is periodic in the (x, y) plane. The thermopower is calculated along the temperature gradient which is taken to be perpendicular to the interface.

using the temperature-dependent Seebeck coefficients for the two magnetic configurations $S_{\mathrm{P}}(T)$ and $S_{\mathrm{AP}}(T)$. Since $S_{\mathrm{AP}}(T)$ and $S_{\mathrm{P}}(T)$ may differ not only in magnitude, but also in sign, one can imagine that the magnetic contrast in a thermoelectric measurement, as expressed by the MTP ratio, may become larger than the MC ratio for a specific sample. Such an expectation could be confirmed experimentally, for example by Gravier *et al* [9]. In multilayered Co/Cu nanowires these authors found an MTP ratio of −30%, larger than the 20% measured GMR ratio. This behaviour is usually traced back to the fact that the conductance (equivalently, the conductivity σ) is essentially a Fermi surface related property. The thermoelectric voltage (or the Seebeck coefficient), on the other hand, is a measure of the energy dependence of the relaxation rate near the Fermi energy E_{F} [4]. As expressed by Mott's formula [13], the Seebeck coefficient is proportional to the logarithmic derivative of $\sigma(E)$:

$$S = -\frac{\pi^2}{3e} k_{\mathrm{B}}^2 T \left.\frac{\mathrm{d}\ln\sigma(E)}{\mathrm{d}E}\right|_{E=E_{\mathrm{F}}}, \tag{3}$$

where e and k_{B} are, respectively, the elementary charge and the Boltzmann constant. On the basis of equation (3), one could derive a rather simple relation between the two quantities, the MTP and the MC ratios [8].

Phenomenological models, while useful in identifying general trends, do miss the important link between the described quantity and the underlying electronic structure. Precisely the opposite philosophy is adopted in first-principles based investigations, such as the ones presented here, which perform appropriate modifications of the electronic structure and track the evolution of a given property with the ultimate purpose of achieving specific design rules for a desired target value.

For this purpose, we have considered one of the GMR prototypes, the Co/Cu multilayered system. Many of its ground-state properties as well as the CIP- or CPP-GMR effects have been already addressed on an *ab initio* level [14–24]. In contrast, first-principles calculations of the magneto-thermoelectric properties of several Co/Cu heterostructures, which require a significantly larger computational effort, have only recently gained increased attention [25, 26].

The multilayered structure subject to our investigations can be seen as a stacking of $\mathrm{Co}_m/\mathrm{Cu}_q$ bilayers of thickness m and q embedded in Cu(001). Accompanying the variations in the metallic layer thickness, the number of repeats N was also treated as a variable, leading to the actual configuration $\mathrm{Cu}[(N-1)(\mathrm{Co}_m/\mathrm{Cu}_q)/\mathrm{Co}_m]\mathrm{Cu}$, as schematically shown in figure 1(b). Note that, by construction, N was taken as finite, that is, no periodic boundary conditions along the (001) growth direction were imposed. The transport properties of these systems are investigated by performing first-principles calculations of the underlying electronic structure by means of a spin-polarized relativistic Green's function method [27–29]. The results obtained for the conductance and the Seebeck coefficient in a CPP geometry—the temperature gradient taken perpendicular to the interface—are analyzed in view of the modifications in the electronic structure induced by varying the morphology of the heterostructure, either through the number of repeats N or of the thickness $m(q)$ of the constituent Co (Cu) layers.

The close lattice match of Co and Cu, as well as the advanced fabrication technique of the nanopillars by electrodeposition, allows researchers to build stacks with a large number of Co repeats. If the dominating scattering mechanism of the electrons is scattering by the Co/Cu interfaces, it is to be expected that the resistivity of a stack increases with the number of repeats N, while the MC ratio is almost independent of N. For the Seebeck

coefficient, which has the physical meaning of a voltage, its dependence on N is not obvious. Our calculations show that both $S(T)$ and the MTP ratio converge rather rapidly with the number of Co repeats in the Co/Cu stacks, with reasonably converged values being attained already at $N = 4$.

A modulation of the electronic density of states due to quantum confinement effects in ultra-thin layers may affect the resistivity, but to an even higher degree the Seebeck coefficient of multilayered structures. Quantum well states (QWSs) were found to lie at the origin of an oscillatory behaviour observed for many physical properties of these systems, ranging from interlayer exchange coupling [14, 15, 30] to magnetic anisotropy energy [20]. While in most of the cases this non-monotonic manifestation was ascribed to QWSs occurring in the non-magnetic spacer, both theoretical [31–33] and experimental [34] investigations evidenced the important role played by the ferromagnetic layer.

We have recently investigated the Seebeck magnetic anisotropy in Cu/Co_m/Cu trilayers [25] and determined that its value may become very large for thin Co layers. Our calculations have shown that minority spin QWSs formed in the ferromagnetic Co layers hybridize with a high-mobility band crossing the Fermi energy contributing to a large, thickness-dependent sensitivity of the Seebeck coefficient on the orientation of the magnetization [25].

Here we show that, owing to the same QWS–p-band complex, strong variations in the amplitude and sign of both the Seebeck coefficient and the MTP occur in multilayers consisting of Co stacks of up to seven monolayers. For the design of Cu/Co stacks for MTP read-out, this would mean that depositing a small number of Co layers with precise control of the layer thickness is more useful than increasing the number of Co repeats in the stack. By comparison, the Co and Cu thickness dependence of conductance and MC ratio was found to be much weaker.

The paper is organised as follows. We start by providing the relevant computational details, including the geometry of the systems, in section 2. Section 3 deals with the particular case of a single Co layer embedded in Cu (001), in which we mostly focus on aspects of the electronic structure, with particular attention paid to the quantum well states appearing in the Co layer. The last two sections are devoted to the transport properties of the Cu[$(N-1)$(Co_m/Cu_q)/Co_m]Cu multilayers, with detailed discussions on their N-, m-, and q-dependence.

2. Geometry of the system and theoretical background

The calculations for the Cu[$(N-1)$(Co_m/Cu_q)/Co_m]Cu multilayer systems were performed using a spin-polarized relativistic (SPR) [29, 35] version of the screened Korringa–Kohn–Rostoker Green's function (KKR-GF) method [36–38]. We apply the same procedure as described in our previous investigations on the Cu/Co_m/Cu trilayers [25], which essentially consists of three steps: (i) setting up the geometry of the system; (ii) the self-consistent determination of the ground state potentials; and (iii) using these as input for the transport calculations which are based on the Landauer–Büttiker formula as implemented in the KKR-GF method [39, 40] within a relativistic representation [27, 28]. Our approach, discussed to some extent in this section, has the one-electron retarded Green's function $G^+(\vec{r}, \vec{r}\,'; \varepsilon)$ at energy $\varepsilon = E + i\delta$ as central quantity.

2.1. Modelling the multilayered systems

We model the systems under investigation by taking two half-infinite Cu leads with an interaction region inserted in-between, all sharing the same in-plane two-dimensional (2D) periodic lattice. Since the natural lattice misfit between elemental Co and Cu is rather small (less than 2%), we neglect the lattice relaxation at the interfaces and take all atomic positions as being fixed to the ideal (001)-stacked fcc lattice with the lattice constant equal to the experimental fcc-Cu value of 3.61 Å. The interaction region contains the [$(N-1)$(Co_m/Cu_q)/Co_m] multilayered structure and up to 10 atomic monolayers (MLs) of Cu on both sides. These additional Cu MLs are meant to ensure a smooth transition towards the Cu leads.

Schematic representations of selected setups for the interaction region are provided in figure 1(b) for varying number of Co repeats (here, $N = 2$ and $N = 3$) and individual Co ($m = 4$ and $m = 6$ ML) and Cu ($q = 4$ and $q = 8$ ML) layer thickness. For our investigations we had considered, changing just one variable at a time, $N = 1, \ldots, 6$ and combinations of m and q ranging between 4 and 8 MLs thickness. We have determined the longitudinal thermopower occurring under a temperature gradient taken parallel to the growth direction z. Note that along this direction, no periodic boundary conditions are imposed. We furthermore emphasize that different numbers of repeats effectively mean differently sized finite objects along z; an increase in N (at a given m and q) is equivalent to an increase in the thickness of the interaction region.

2.2. Electronic structure calculations

For each of the configurations, the potentials are determined self-consistently using the screened KKR-GF method [29], considering spherical potentials in the atomic sphere approximation (ASA) within the local spin-

density approximation in the Vosko, Wilk and Nussair parametrization [41]. An angular momentum cut-off of $l_{\max} = 3$ was taken for the Green's function expansion.

In a preliminary step, a separate self-consistent calculation is performed in order to determine the potential of the two (identical) half-spaces left and right of the interaction region. A second self-consistent procedure is applied to the interaction region itself, in which all its potentials are iterated, whereby the outer-most Cu potentials asymptotically match the ones in the lead. This matching is accomplished by means of the decimation technique [42], in which the lead potentials determined in the first step provide the appropriate boundary conditions of the heterostructure. Different magnetic couplings between adjacent Co layers, parallel and anti-parallel, were separately considered at each $(N,\ m,\ q)$ combination. The collinearity of the spin magnetic moments was the only constraint imposed *a priori*.

As a consequence of the 2D-periodicity of the layered system, the Green's function can be Fourier transformed in a 2D representation with the Bloch vector $\vec{k}_{\parallel}$ as constant of motion and retaining an index i for the position along the growth direction z. Within the KKR-GF scheme, the Green's function is expressed in terms of the matrix $\underline{G}^{ij}(\vec{k}_{\parallel},\ \varepsilon)$. This matrix describes the propagation of the electron wave between the atomic sites i and j at positions $\vec{R}_i, \vec{R}_j$ and is labelled, in our adopted representation, by the relativistic quantum numbers $\Lambda = (\kappa,\ \mu)$, i.e. $(\underline{A})_{\Lambda\Lambda'} = A_{\Lambda\Lambda'}$ [29]. Let us note here that since in a relativistic formulation the spin is not a constant of motion, each state may acquire different amounts of spin up and down character. For this reason, we shall use the designation majority/minority spin rather than up/down (↑/↓).

2.3. Transmission probability, conductance and the Seebeck coefficient

Combining the structural Green's function matrix calculated for a given 2D-periodic system with the matrices $\underline{M}^i, \underline{M}^j$ of the z-component of the relativistic current operator at sites i and j enables the calculation of the electronic transmission probability between two atomic planes I and J according to the expression [28]:

$$\mathcal{T}\left(\vec{k}_{\parallel},\ E\right) = \sum_{i\in I, j\in J} \mathrm{Tr}\left[\underline{M}^{i\dagger}\underline{G}^{ij}\left(\vec{k}_{\parallel},\ \varepsilon\right)\underline{M}^{j}\underline{G}^{ij\dagger}\left(\vec{k}_{\parallel},\ \varepsilon\right)\right], \tag{4}$$

where each 2D vector $\vec{k}_{\parallel}$ can be seen as a conduction channel [40]. By integrating over the 2D Brillouin zone (2D-BZ) the total transmission probability $\mathcal{T}(E)$ at energy E is then [40]:

$$\mathcal{T}(E) = \frac{1}{A_{\mathrm{2D-BZ}}}\int_{\mathrm{2D-BZ}} \mathrm{d}^2\vec{k}_{\parallel}\,\mathcal{T}\left(\vec{k}_{\parallel},\ E\right). \tag{5}$$

In the case of a weak spin–orbit coupling, as it is the case for the light 3d transition metals, Popescu *et al* [27, 28] could show that the transmission through the 'fully relativistic resistor' expressed by equation (4) can be approximated by $\widetilde{\mathcal{T}}(\vec{k}_{\parallel},\ E)$:

$$\begin{aligned}\mathcal{T}\left(\vec{k}_{\parallel},\ E\right) \simeq \widetilde{\mathcal{T}}\left(\vec{k}_{\parallel},\ E\right) = \widetilde{\mathcal{T}}_{\uparrow\uparrow}\left(\vec{k}_{\parallel},\ E\right) + \widetilde{\mathcal{T}}_{\downarrow\downarrow}\left(\vec{k}_{\parallel},\ E\right)\\ + \widetilde{\mathcal{T}}_{\uparrow\downarrow}\left(\vec{k}_{\parallel},\ E\right) + \widetilde{\mathcal{T}}_{\downarrow\uparrow}\left(\vec{k}_{\parallel},\ E\right)\end{aligned} \tag{6}$$

which provides a spin decomposition essentially equivalent to the Mott two-current model. Equation (6) can be regarded as its generalization to the relativistic case. In addition to the spin-conserving (↑↑ and ↓↓) channels, it also includes spin-mixed ones (↑ ↓ + ↓ ↑), induced by the spin–orbit coupling. We will use this approximate spin decomposition only for a qualitative discussion in section 3.1.

Following Sivan and Imry [43], the Seebeck coefficient $S(T)$ can be obtained from $\mathcal{T}(E)$ through the expression

$$S(T) = -\frac{1}{eT}\frac{\int \mathrm{d}E\ \partial_E f_0\ \mathcal{T}(E)\left(E - E_{\mathrm{F}}\right)}{\int \mathrm{d}E\ \partial_E f_0\ \mathcal{T}(E)}, \tag{7}$$

where $f_0 \equiv f_0(E,\ T,\ \mu)$ is the Fermi–Dirac distribution function at energy E, temperature T, and chemical potential μ, while $\partial_E f_0 = \partial f_0/\partial E$ represents its energy derivative. The denominator in the last equation is related to the temperature-dependent conductance $g(T)$ by:

$$g(T) = -\frac{e^2}{h}\int \mathrm{d}E\ \partial_E f_0\ \mathcal{T}(E). \tag{8}$$

The various parameters involved in the actual evaluation of these quantities were chosen in the following way. For the 2D-BZ integral required for the transmission probability, equation (5), a regular $1000 \times 1000\ \vec{k}_{\parallel}$ -grid was found necessary to achieve convergency of $\mathcal{T}(E)$ over a broad range of energy arguments. For the integrals in equations (7) and (8), on the other hand, $\mathcal{T}(E)$ was explicitly calculated on a 1 mRy-spaced regular mesh, then interpolated on a denser mesh of 0.1 mRy. In these equations, the limits of the energy interval below

and above E_F were set in such a way that $\partial_E f_0(E_{min/max}) < 10^{-8}$, a limit found to be more than sufficient in providing well-converged results.

2.4. Explicit temperature-dependent effects

The formalism employed here rigorously describes elastic scattering at the interfaces and treats the simultaneous occurrence of spin polarization and relativistic effects, such as spin–orbit coupling, on equal footing. Temperature enters in this approach through the Fermi–Dirac distribution function, but temperature-dependent scattering, e.g. by atomic vibrations or spin fluctuations, are neglected.

Inclusion of atomic displacements at finite temperature in transport properties calculations within *ab initio* methods has been recently accomplished by treating them as static disorder via the coherent potential approximation (CPA) [44]. Alternatively, one could use large 2D supercells and apply a frozen phonon approach averaging over explicit different atomic displacements. We note, however, that $S(T)$ is the quotient of two integrals involving the transmission probability $\mathcal{T}(E)$. As such, since it appears both in the numerator and the denominator, any additional temperature dependence due to inelastic scattering exhibiting only a weak energy dependence will tend to partially cancel out.

Accounting for electron scattering by spin fluctuations in various ferromagnetic metals and alloys has been convincingly demonstrated to improve the agreement between calculated and experimentally determined temperature-dependent resistivity [45, 46]. More recently, Kováčik *et al* [26] investigated the effect of spin disorder induced elastic scattering processes on the magneto-thermoelectric phenomena of several nano-structured Co/Cu systems. These authors could show that, while the spin-dependent electron scattering does indeed influence the spin-caloric transport coefficients at elevated temperatures, the way in which it manifests itself is strongly case dependent. In particular, no general trends could be identified; neither do quantitative nor qualitative predictions appear to be possible without an explicit calculation [26]. To what extent inelastic scattering on spin fluctuations influences the Seebeck coefficient is hardly explored. It may be noted that Piraux *et al* [3] invoked inelastic spin-dependent electron–magnon scattering to explain the increase in the MTP at high temperatures observed experimentally in Co/Cu and Fe/Cu thin multilayers. However, as we will show below, an equally large MTP can be obtained accounting solely for the electronic structure contributions to the thermopower. For systems with a gapped band structure, such as magnetic half-metals or tunnel junctions, modifications of the electronic properties due to dynamic spin fluctuations at finite temperatures have been addressed via phenomenological models [47, 48] or via dynamical mean field theory (DMFT) [49]. For systems as large as those considered here, such an advanced many-particle treatment is computationally not feasible at present.

The importance of these temperature-dependent effects notwithstanding, our primary focus here is to identify the specific effects on the magneto-thermopower which are intimately connected with the electronic structure and are solely induced by quantum confinement. As such, properly accounting for the effects discussed above is well beyond the purpose of the current investigations, although this is clearly needed in future studies for an improved quantitative agreement with the experiment.

3. A single Co layer embedded in Cu(001)

We begin our discussion by presenting results obtained for a single Co layer embedded in Cu(001), a geometry setup corresponding to $N = 1$ in the general notation Cu$[(N-1)(\mathrm{Co}_m/\mathrm{Cu}_q)\mathrm{Co}_m]$Cu introduced above. We shall first analyze briefly the electronic structure in the proximity of the Cu/Co interface and illustrate how its peculiarities are reflected in the transmission probability for a single Co layer of varying thickness m. The $\mathcal{T}(E)$ transmission profile for $m = 4$ will be shown to exhibit a peak in the minority spin channel immediately below the Fermi energy. This peak is intimately connected with a complex formed by a quantum well state (QWS) and a high mobility p-band present in the interface layers, with which the QWS hybridizes. These findings for the single layer system will be important in understanding the transport properties of the multilayered Cu$[(N-1)(\mathrm{Co}_m/\mathrm{Cu}_q)/\mathrm{Co}_m]$Cu systems.

3.1. Density of states and transmission probability

Electronic structure calculations performed on the Co/Cu systems [14, 18, 23, 24] revealed that the majority spin d-band is completely filled and the energy range at and near the Fermi level is dominated by the 3d minority spin states stemming from the Co. These features are accordingly reproduced by our calculations and reflected in the spin-resolved density of states (DOS) for the Cu/Co_4/Cu trilayer system shown in figure 2(a). Here the DOS is further projected on the Co and Cu atoms in the vicinity of the Cu/Co interface as well as on their angular momentum (s+p)- and d-components.

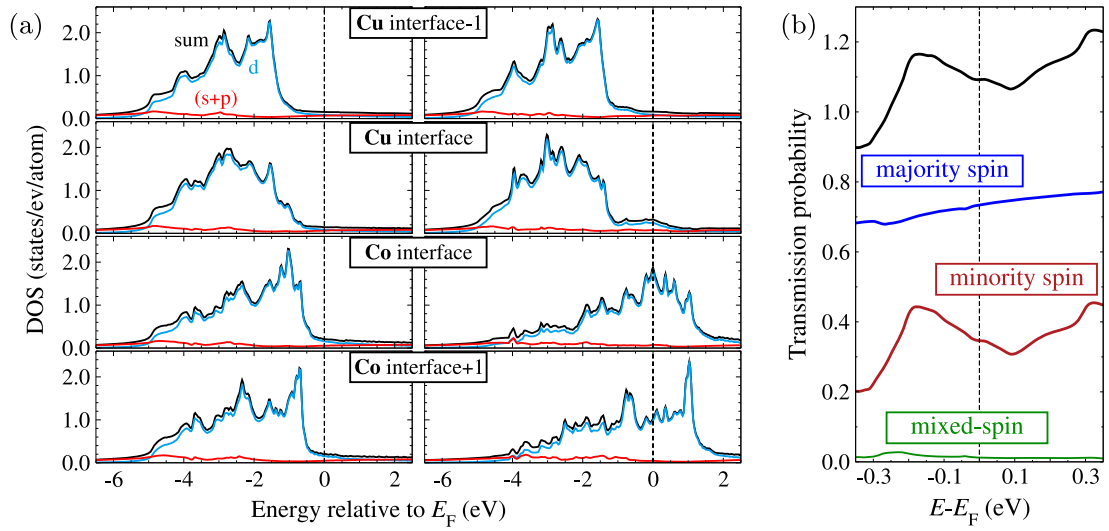

Figure 2. (a) Spin- and angular momentum resolved local DOS projected on the Cu and Co atoms in the vicinity of the Cu/Co interface, with the majority (minority) spin channel in the left (right) panels. The (s+p)-DOS are shown as sum (red lines) while the d-DOS (light blue) is seen to have the dominant contribution to the total DOS (black). (b) Electronic transmission probability in the Cu/Co_4/Cu trilayer system. The total transmission (black) is decomposed in its spin-conserving (blue and dark red) and spin-mixing (green) components. Note the pronounced peak in the minority spin transmission at about −0.2 eV. The Fermi energy, set by the Cu leads, is taken as reference in this figure.

Figure 2(a) evidences that the d-DOS (light blue curve) of both Co and Cu has an overwhelming contribution to the total DOS of the Co/Cu heterostructure in both spin channels. We further note the large Co-related contribution in the minority spin channel in the proximity of the Fermi energy, contrasting with the extremely reduced DOS on the Cu sites. Only the first Cu layer near the interface exhibits a slight spin polarization, induced by its neighbouring Co atoms.

The dominant d-character of the minority spin states close to the Fermi energy is accordingly reflected in the transport properties. Indeed, the d-states are characterized by a stronger localization and a reduced mobility as compared to the s- and p-states. We show in figure 2(b) the transmission probability $\mathcal{T}(E)$ for the same Cu/Co_4/Cu trilayer system, containing a 4 ML thick Co layer. The black curve in this figure represents the total transmission, calculated for various energy arguments E using equation (5). Applying the spin decomposition leading to the approximate form (6) allows us to identify the spin-conserving and spin-mixing transmission channels in $\mathcal{T}(E)$. As a result of the rather small spin–orbit coupling, the spin-mixing transmission (green lines) is negligibly small. In spite of a small DOS near E_F, the largest transmission component is the spin-conserving majority one. The minority spin transmission is only about one third of the total. Nevertheless, while $\widetilde{\mathcal{T}}_{\uparrow\uparrow}(E)$ is nearly featureless and shows a weak variation with E, it is the $\widetilde{\mathcal{T}}_{\downarrow\downarrow}(E)$ component which modulates the full transmission profile $\mathcal{T}(E)$. This different qualitative behaviour arises from the different character of the states involved in the transmission through the various channels: nearly exclusively s- and p-states for the majority spin, hybrid s–p and d-states for the minority spin. The first important conclusion of our investigations can thus be formulated as follows. Although comparatively small in magnitude, the minority spin transmission is expected to be much more sensitive to the morphology of the system. Changes in the transport properties caused by geometry modifications can be traced back nearly exclusively to modifications in the minority spin electronic structure.

While the general characteristics of the transmission profile discussed above were found to be valid for all the systems investigated, the pronounced peak in the minority spin transmission (dark red line in figure 2(b)), 0.2 eV below the Fermi energy, is a peculiarity of the chosen Co thickness, $m = 4$ ML. It represents, in fact, a signature of a QWS arising in the minority spin band of Co. A detailed discussion of these QWSs is the subject of the next section.

3.2. Quantum well states

The appearance of QWSs in the Co slab has been found responsible for the non-monotonic behaviour of the magnetic anisotropy energy (MAE), evidenced both experimentally [19] and theoretically [20] in the Cu/Co_m/Cu trilayers, as well as for the oscillations in the interlayer exchange coupling occurring in Co/Cu for thin Co

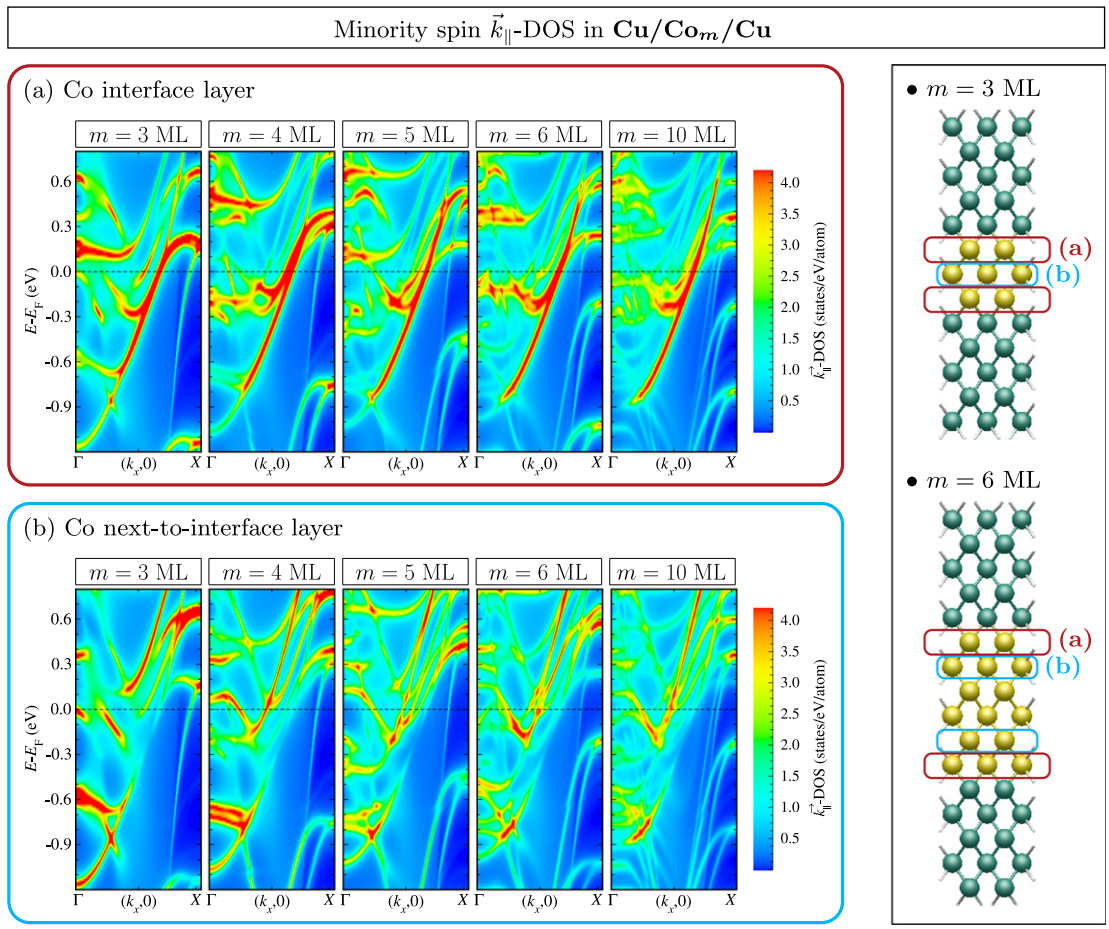

Figure 3. Minority spin $\vec{k}_{\parallel}$-resolved DOS projected on the (a) interface and (b) next-to-interface Co atom in the Cu/Co$_m$/Cu trilayer system for various values of m, as shown schematically on the right side of the figure. For the interface layer (a) typical signatures of QWSs appearing as flat bands above (odd m) and below (even m) E_F for thin Co slabs as well as a p-type band crossing the Fermi energy E_F (taken here as reference value) can be recognized. The latter has only a weak correspondent in the next-to-interface layer (b). Note that the same scale has been used in both panels.

layers [17]. In a recent study of the authors [25], the QWSs were also shown to play an important role in inducing an anisotropic MTP in the same systems. In particular, we identified a hybrid complex formed by the QWSs and a p-type band specific to the Co/Cu interface. These hybrid states provide extremely efficient channels for the minority spin electrons, as evidenced by the aforementioned peak, 0.2 eV below E_F, in Cu/Co$_4$/Cu. In the next sections we shall link our findings for the Seebeck coefficient and the MTP precisely to these peculiarities of the electronic structure.

The minority spin channel QWSs appearing in the Co slab have been investigated by calculating the angular momentum and atom projected Bloch spectral function (BSF) $A_i(\vec{k}_{\parallel}, E)$ [29]:

$$A_i\left(\vec{k}_{\parallel}, E\right) = -\frac{1}{\pi N}\,\mathrm{Im\,Tr}\sum_{n,n'}^{N} e^{i\vec{k}_{\parallel}\left(\vec{\chi}_n - \vec{\chi}_{n'}\right)} \times \int d^2 r_{\parallel}\, G\left(\vec{r}_{\parallel} + \vec{R}_i + \vec{\chi}_n, \vec{r}_{\parallel} + \vec{R}_i + \vec{\chi}_{n'}; E\right), \tag{9}$$

where $\vec{\chi}_n, \vec{\chi}_{n'}$ are translation vectors of the 2D periodic lattice, $\vec{r}_{\parallel} = (r_x, r_y, 0)$, and $\vec{R}_i = (0, 0, z_i)$ represents the z-coordinate of the ith atom. The BSF is a quantity that can be regarded as a $\vec{k}_{\parallel}$-resolved DOS.

Figure 3 depicts the minority spin component of $A_{\mathrm{Co}}(\vec{k}_{\parallel}, E)$ projected on the first (panel (a)) and second (panel (b)) Co atomic layers near the Cu/Co interface, with the respective location of each layer schematically drawn at the side of the figure. The different frames in each panel follow the variation of the Co layer thickness m MLs in the Cu/Co$_m$/Cu trilayer system. Such E versus $\vec{k}_{\parallel}$-type plots allow us to identify the projected band structure in the 2D-BZ, a picture familiar from angle-resolved photo-emission experiments.

The formation and appearance of a certain QWS will depend on the Co thickness m, alternating between odd and even number of MLs. For a given parity, on the other hand, the m-dependence is reflected in a variation in

the energy position of the QWSs. Typical signatures of QWSs can be observed as flat bands in the BSF of the interface Co layer (panel (a)) near the 2D-BZ centre: (i) around 0.15 eV for $m = 3$ and $m = 5$ and (ii) around −0.2 eV and 0.4 eV for $m = 4$ and $m = 6$, energy values relative to the Fermi level. With increased thickness of the Co slab, the QWSs morph into a continuum, as seen in the right-most frame of figure 3(a) for $m = 10$ MLs.

The second important aspect revealed by the top panel of figure 3 is the existence of a high-mobility p-band for the minority spin carriers, crossing the Fermi energy. This band, evidenced by the red-coloured, *S*-shaped feature of the BSF in figure 3(a), stems from the Cu and Co atoms adjacent to the interface and exhibits no thickness dependence. In other words, it is an ubiquitous characteristic of the Co/Cu interface.

For the case of an *even* number of MLs *m*, the QWS forming below the Fermi energy will couple to this p-band, leading to the formation of a p–d hybrid complex. This is precisely the origin of the strong transmission evidenced in the minority spin channel at −0.2 eV in figure 2(b) and, as shown below, for the positive value of the Seebeck coefficient associated with $m = 4$ ML Co thick systems. Note that a similar hybrid band complex also appears above the Fermi energy, at 0.45 eV. This is however too far to contribute to the integrand of equation (7).

It is easy to see how the morphology of the system may have significant influence on its electronic structure, and, as a result, on its transport properties. By comparing the spectral functions of the two different Co atoms in figures 3(a) and (b) (displayed on an identical scale) one can see, for the next-to-interface layer, a strong reduction in the amplitude of the p-band–related BSF below the Fermi energy. Thus, for the transmission channels opened by the QWS–p-band complex it will mean that their weight and importance in the total transmission will diminish with increasing Co thickness. This effect is further amplified by the smearing out of the QWSs. When *m* is *odd*, on the other hand, the QWS appearing above the Fermi energy couples very weakly, if at all, with the highly mobile p-band. As a consequence, no corresponding high energy transmission peak is expected for odd *m*. This thickness-triggered filtering of the transmission channels involved in the conduction was found responsible for the non-monotonic behaviour of the Seebeck coefficient in Cu/Co_m/Cu trilayers [25].

Additional variables come into play in the case of multilayered systems. The size of the Cu spacer placed between the Co layers will modify the way in which the different states will or will not couple across the interfaces, leading to an enhancement or suppression of various transmission channels. Likewise, a varying number of Co and Cu repeats may further complicate the picture. Furthermore, when different magnetic alignments between adjacent Co layers are considered, one has to bear in mind that the minority/majority spin channels get swapped. We discuss these aspects in the next sections, essentially showing that a broad range of values may arise for both the Seebeck coefficient and the MTP, depending on the different morphological parameters.

4. Varying number of Co repeats

In the previous section the discussion focused on electronic structure characteristics related to a single Co layer of varying thickness embedded in Cu(001). We have analyzed how these may influence directly the transmission probability and, through it, the various transport properties. The first question to ask is how much and to what extent the knowledge gained so far is transferable to the multilayered Cu[$(N-1)(Co_m/Cu_q)/Co_m$]Cu systems. In this section we discuss results obtained by modifying the number of Co repeats *N* while keeping the other parameters, *m* and *q*, fixed. For convenience and easier comparison with the results already presented, we restrict the discussion, without losing any generality, to the case $m = q = 4$ MLs. The most important conclusions drawn at the end of this section are: (i) the electronic structure features present in the single-Co layer system transfer to the Co-stacked systems; (ii) increasing the number of Co repeats reduces the transmission through the heterostructure without, however, significantly modifying its *E*-dependent profile; and (iii) at high temperatures, the Seebeck coefficients, both for parallel and anti-parallel alignments, as well as the derived MTP, are reaching converged values in *N* rather fast.

4.1. Electronic structure and transmission probability

The electronic structure calculations performed for the Cu[$(N-1)(Co_m/Cu_q)/Co_m$]Cu systems with $N = 1, \ldots, 6$ revealed an interesting feature: the calculated ground state properties such as spin and orbital magnetic moments, DOS or BSF curves projected on the individual components exhibit a rather weak dependence on *N*. As an illustrative example we show in figure 4(a) the spin magnetization profiles for $N = 1$ (red bullets) and $N = 2$ (dark blue crosses), that is, one and two Co slabs embedded in Cu, each of a thickness $m = 4$ MLs. For $N = 2$ the two Co layers are separated by a thin Cu spacer ($q = 4$ MLs). One can see that there are hardly any differences noticeable in the individual spin magnetic moments on the Co atoms in the two cases, Cu/Co_4/Cu and Cu/$Co_4Cu_4Co_4$/Cu. Specifically, for the Co atoms nearest to Cu, the spin magnetic moments obtained were (in Bohr magnetons μ_B): 1.6137 ($N = 1$), 1.6134 ($N = 2$, outer Co), and 1.6130 ($N = 2$, inner Co). In spite of

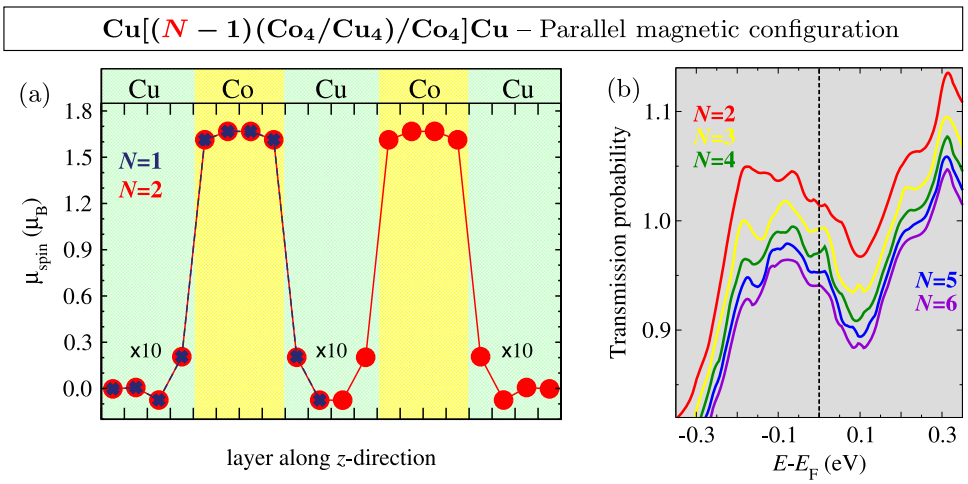

Figure 4. (a) Spin magnetization profile of the $Cu/Co_4Cu_4Co_4/Cu$ system ($N = 2$, red bullets) with a parallel (P) magnetic configuration as compared to that of the $Cu/Co_4/Cu$ trilayer ($N = 1$, dark blue crosses). The figure emphasizes the quasi-independence of the spin magnetic moments in the Co layers on the number of repeats N. Note that the values corresponding to the Cu atoms are multiplied by a factor of 10. (b) N-dependence of the electronic transmission probability $\mathcal{T}(E)$ in $Cu[(N-1)(Co_4/Cu_4)/Co_4]Cu$ with a P-alignment of the Co magnetic moments. The transmission curves are shown around the Fermi energy E_F, taken here as reference in the same range as in figure 2(b).

the very small thickness of the spacer, the individual Co layers obviously display the same properties, regardless of N. Analogous results were obtained for the other number of repeats; furthermore, the Cu spacer layers of equal thickness also exhibit similar characteristics.

In other words, these findings imply that all the considerations made in the previous section regarding the electronic structure of a single Co slab transfer to the multilayered systems, qualitatively completely and quantitatively to a large extent. This also holds, in particular, for the QWSs formation and the Co/Cu-interface specific p-band in the minority spin channel.

Not surprisingly, a similar one-to-one transferability holds only partly in the transmission probability profiles. These are shown in figure 4(b) for $m = q = 4$ MLs, $N = 1, \ldots, 6$, and with all the magnetic moments oriented parallel to one another. Note that throughout the next figures we will use the same colour-coding convention, borrowed from the solar spectrum: as the variable under investigation increases, the colours used in the graphical representation change from red to purple. The general trend that can be recognized from figure 4(b) is an overall down-scaling of the $\mathcal{T}(E)$ profiles with increasing N. This is a direct consequence of successively adding interfaces, that is, electron scattering sources, to the transmission process between the left and right leads. It is nevertheless obvious that the reduction in transmission is not a uniform function of energy argument. For this reason, the peak at −0.2 eV discussed above for $N = 1$, although still present for all values of N, appears of varying shape and width. We also point out the slope of $\mathcal{T}(E)$ near the Fermi energy, which is changing sign with N. While being the result of subtle variations in the way different states couple, these changes influence the thermoelectric properties of the multilayered system only in the limit of low temperatures.

4.2. Spin-dependent thermally induced transport properties

Figure 5(a) displays the dependence of the Seebeck coefficient on the number of Co repeats N in the multilayered $Cu[(N-1)(Co_4/Cu_4)/Co_4]Cu$ systems. The two panels correspond to results obtained for two magnetic configurations, a parallel (P) and an anti-parallel (AP) alignment. The latter is understood as the succession of Co slabs, each of m MLs thickness (here $m = 4$), in which the magnetic moments in one slab are opposed to those of its neighbouring Co slabs. As an example, for $N = 5$ one would have for the Co slabs the arrangement (↑↑↑↑↑) for the P-alignment and (↑↓↑↓↑) for AP.

As mentioned in the introduction, measurements of the Seebeck coefficient are usually interpreted on the basis of Mott's formula, equation (3), which provides a direct link between $S(T)$ and the conductivity $\sigma(E)$ of a sample. Its range of validity has been discussed to some extent in the literature, e.g. by Jonson and Mahan [50], who showed that it gives the correct $T \to 0$ behaviour for independent electrons interacting with static impurities and for adiabatic phonons. Beyond Mott's formula, the way in which a transmission probability profile $\mathcal{T}(E)$ influences the sign and size of the Seebeck coefficient at finite T can be understood on the basis of equation (7). In this equation, a temperature increase effectively extends the integration range, by increasing the non-zero width of $\mathcal{T}(E)(\partial f_0/\partial E)$. Because of the $(E - E_F)$ term, the numerator may be seen as a centre of mass

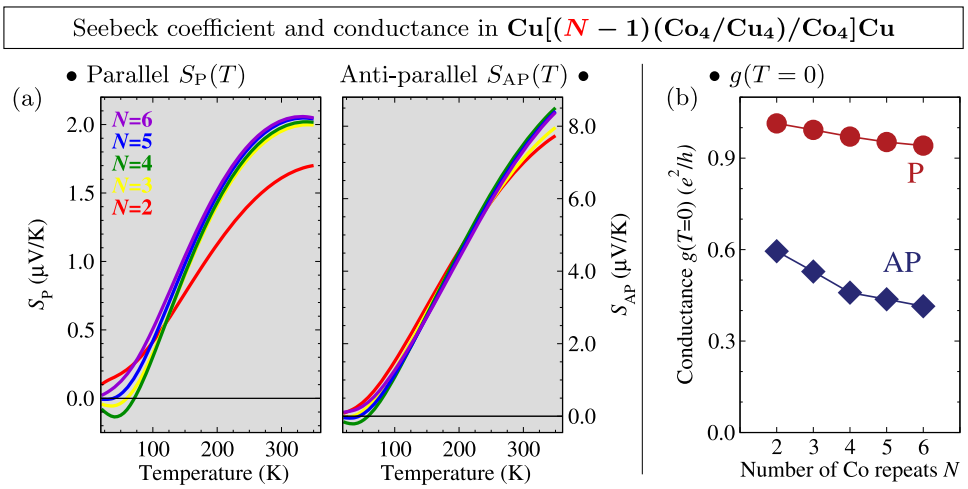

Figure 5. Dependence of (a) the Seebeck coefficient $S(T)$ and (b) the zero temperature conductance $g\,(T=0)$ on the number of Co repeats N in the Cu$[(N-1)(\mathrm{Co_4/Cu_4})/\mathrm{Co_4}]$Cu multilayered systems: (a) $S_P\,(T)$ for parallel (P, left panel) and $S_{AP}\,(T)$ for anti-parallel (AP, right panel) alignment of the magnetization in the Co layers. (b) Conductance for P (bullets) and AP (diamonds) alignments. Note the different scale used for $S_P\,(T)$ and $S_{AP}\,(T)$.

of $\mathcal{T}\,(E)\,(\partial f_0/\partial E)$ [51]. Consequently, both sign and value of $S(T)$ will be sensitive even to small changes in the numerator's integrand below or above E_F.

Finally, we note that, in terms of the transmission probability $\mathcal{T}\,(E)$, Mott's formula can be obtained as the $T \to 0$ limit of equation (7) and translates into $S(T)$ being positive (negative) for a negative (positive) slope of $\mathcal{T}\,(E)$ near the Fermi energy. In other words, a large transmission below (above) E_F will result in a positive (negative) $S(T)$. Due to this peculiarity, the Seebeck coefficient measurement is a well-known tool in establishing the nature of carriers, p- or n-type, in semiconductors.

The above considerations provide the basis on which to understand the Seebeck coefficient results, in conjunction with the transmission probability profiles depicted in figure 4(b). In both magnetic configurations, $S_P\,(T)$ and $S_{AP}\,(T)$ exhibit a non-monotonic behaviour at low temperatures, consistent with the changes in the slope of $\mathcal{T}\,(E)$ near the Fermi energy observed in figure 4(b). These results are consistent with Mott's formula. At increased temperatures, both $S_P\,(T)$ and $S_{AP}\,(T)$ become and remain positive, with $S_{AP}\,(T)$ much larger (about a factor of four) than $S_P\,(T)$. This positive sign is a direct consequence of the enhanced transmission in the range of 0.2 eV below the Fermi energy, stemming from the minority spin carriers, as discussed above. It is, as we have seen, the thermoelectric signature of the QWS–p-band complex present in the Co slabs of thickness $m = 4$ MLs.

Figure 5(a) further shows that, above $T \simeq 100$ K, the Seebeck coefficient converges rather fast with the number of Co repeats N, for both magnetic alignments. Mathematically, the fast convergence of $S_{P/AP}\,(T)$ with N results from its definition as a quotient of two integrals. The behaviour is clearly different for the $T = 0$ K conductance $g\,(T=0)$ which is shown in figure 5(b) for the same systems and magnetic configurations. Note that, for clarity, we omitted displaying its temperature dependence. For both $g_P\,(T)$ and $g_{AP}\,(T)$ this was found to be quite weak, a similar result being reported by Kováčik *et al* [26].

In order to quantify the magnetic response encountered in the thermoelectric effect, we calculated the MTP ratio according to equation (2). We note that, regardless of the convention adopted for the denominator, one problem might always arise when plotting a temperature-dependent MTP ratio: since the Seebeck coefficient may change sign as a function of T, one will necessarily encounter discontinuities in the graphical representation of the MTP ratio. Such a situation is indeed observed in figure 6, where we present the calculated MTP and MC ratios for the multilayered Cu$[(N-1)(\mathrm{Co_4/Cu_4})/\mathrm{Co_4}]$Cu systems.

As can be seen in this figure, very large and widely spread values for the MTP ratio are predicted in the range of low temperatures. These arise in those areas where S_{AP} approaches zero. Extremely large MTP ratios have been purposefully omitted from the figure. Although not as fast as $S_P\,(T)$ and $S_{AP}\,(T)$, the MTP ratio also attains convergency with N at high temperatures and is in general larger than the MC ratio, a result which is qualitatively consistent with the experimental findings [6, 8, 9]. As was the case for $g_{P/AP}\,(T=0)$, the MC ratio is, in turn, not fully converged with N. We note that a quantitative comparison with the experimental data is not attempted here. The reported results were obtained either for (111)-grown multilayers [6] or for nanowires of ∼10 nm layer thickness [8, 9], much larger than the 4 MLs (6–7 Å) used in our calculations. The effect of the m and q parameters on the (magneto)thermoelectric properties of the Co/Cu multilayers is discussed in the following section.

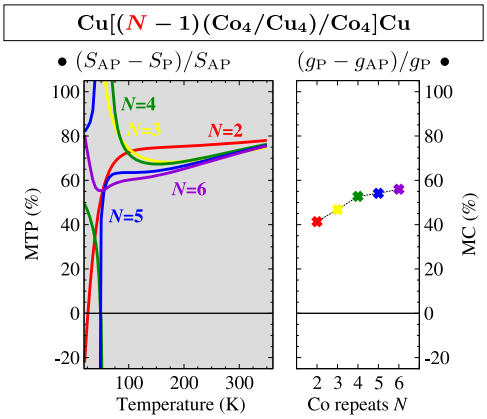

Figure 6. Dependence of the magneto-thermopower (MTP/left) and the zero temperature magneto-conductance (MC/right) on the number of Co repeats N in the Cu[$(N-1)$(Co_4/Cu_4)/Co_4]Cu multilayered systems.

4.3. Interlayer exchange coupling

We close this section by briefly discussing the interlayer exchange coupling in the investigated structures, an electronic structure related issue which is closely connected to the GMR and MTP effects. The functionality of any GMR device relies on its capability of switching, under an applied magnetic field, from an anti-parallel to a parallel coupling of the magnetization in the adjacent ferromagnetic (FM) layers separated by a non-magnetic (NM) spacer. In the absence of an external magnetic field the ground state magnetic configuration is determined by the interlayer exchange coupling (IXC). In many FM/NM heterostructures the IXC was found to exhibit an oscillatory behaviour with the thickness of the NM layer.

The results we obtained for the IXC in Cu[$(N-1)$(Co_m/Cu_q)/Co_m]Cu with varying N, m, and q indicate that an anti-parallel magnetic coupling between the Co layers is only favoured in the range of thin Cu spacers, with an even number, $q = 4$ and $q = 6$, of MLs. This appears to be a common feature for all Co layers, irrespective of their own thickness m and the number of repeats N. Our findings are consistent with previous first-principles investigations of the IXC in Co/Cu bilayers, trilayers or superlattices [14–17]. In particular, we note that all these calculations predict a more stable parallel alignment for thick Cu spacers in the absence of interface roughness [17].

5. Multilayers of varying Co and Cu thickness

In this section we shall study how thickness changes of the individual ferro- and non-magnetic components (the Co and Cu layers) affect the (magneto)thermoelectric properties of the heterostructure. Particular attention will be given to the QWS–p-band hybrid states and their anticipated evolution with the morphology of the system, as suggested by the findings discussed in section 3.

As demonstrated in figure 2(b), for the systems investigated here the transmission is highly spin-conserving. We have also shown that the QWS–p-hybrids are only present in the minority spin band and are characterized by a strong localization at the Co/Cu interface. An increase of either Co or Cu layer thickness is expected to modify the transmission probability profiles through their influence on the transmission channels opened by these states, diminishing their amplitude and weight. In particular, by removing the large contributions to $\mathcal{T}(E)$ below E_F, a corresponding change in sign and increase in absolute value is expected for $S(T)$.

For the results to be presented in the following we keep a fixed number of repeats $N = 4$ in the Cu[$(N-1)$(Co_m/Cu_q)/Co_m]Cu system. We will start our discussion by focusing on the changes induced in the transmission profiles by the modifications in the thickness m and q of the Co and Cu layers and then we will derive the corresponding transport properties. The very general expectations formulated above will be compared with the results provided by the actual calculations. We will show that the values obtained for both the Seebeck coefficient and the MTP span a very broad range, depending on the particular (m, q) combination. Thus, we conclude that, although the expected trends based on 'educated guesses' are generally fulfilled, in most cases explicit calculations are needed in order to make accurate predictions [26, 51].

5.1. The effect of thicker Co and Cu slabs on the transmission probability profiles

When discussing the minority-spin BSFs of a single Co layer in section 3 we emphasized two important aspects: (i) the appearance of QWSs and (ii) the existence of an interface-related, high-mobility p-band. The positions of

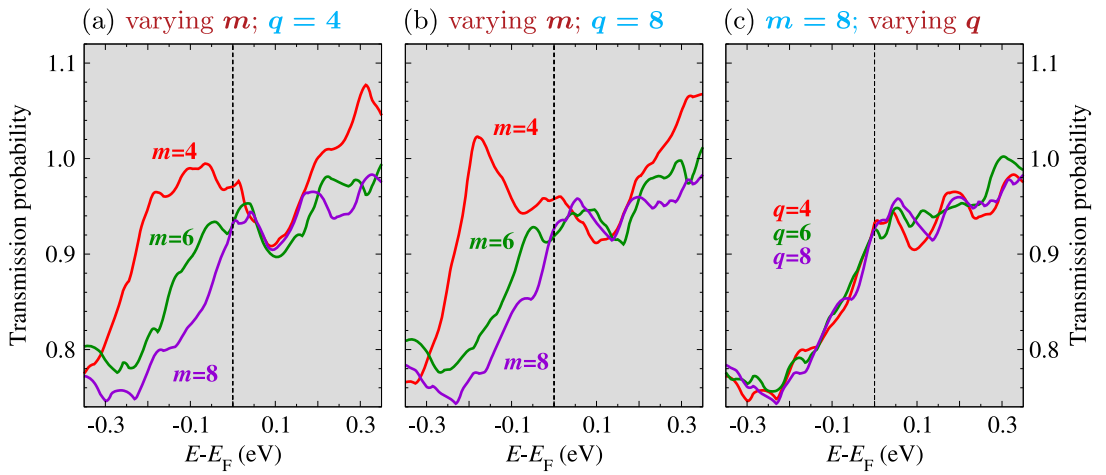

Figure 7. Dependence of the electronic transmission probability $\mathcal{T}(E)$ in Cu[3(Co$_m$/Cu$_q$)/Co$_m$]Cu (number of repeats $N = 4$) on the thickness m and q of the Co and Cu layers: (a) fixed Cu thickness $q = 4$ MLs, varying Co thickness m; (b) fixed Cu thickness $q = 8$ MLs, varying Co thickness m; and (c) fixed Co thickness $m = 8$ MLs, varying Cu thickness q. The magnetic configuration corresponds to a P-alignment of the Co magnetic moments. Transmission profiles for odd number of MLs (m and q) were skipped for the sake of clarity.

the former are obviously thickness dependent but they may hybridize with the latter. As a result, strong transmission channels for the minority spin carriers are opened.

As shown in figure 3, this p-band is ever present, regardless of the Co thickness. The energy position of the QWSs, on the other hand, will change as the Co layer becomes thicker: by a larger extent when m switches from even to odd and only by a smaller amount for $m \rightarrow m + 2k$ (identical parity). Eventually, the QWSs morph into a continuum as the thickness of the Co layers further increases. This evolution of the QWS–p-band hybrids with m must be accordingly reflected in the transmission channels opened by these states.

The results displayed in figure 7 represent a convincing proof that this is indeed the case. Here we show the calculated transmission profiles for Cu[3(Co$_m$/Cu$_q$)/Co$_m$]Cu in the parallel (P) magnetic alignment as a function of either m at fixed q or vice-versa. For the clarity of the picture, the data for an odd number of MLs, otherwise in line with the expected trends, have been omitted. From left to right, the different panels of figure 7 show the changes in $\mathcal{T}(E)$ for (a) $q = 4$ and varying m, (b) $q = 8$ and varying m, and (c) $m = 8$ and varying q. Note that the varying (fixed) quantity in the figure is denoted by dark red (light blue) colours.

Not surprisingly, the thickness dependence of the QWS–p-band complexes discussed above has a significant influence on the transmission probability profiles. The transmission channels connected to these states do follow the expected shifts in position and intensity. As seen in figure 7(a), the increase of the Co layer's thickness from $m = 4$ to $m = 6$ and then to $m = 8$ MLs causes a dramatic drop in $\mathcal{T}(E)$ below E_F. A strong reduction in transmission can also be observed for the high energy peak at 0.3 eV. The direct comparison of the two panels with constant q values (figure 7(a) with $q = 4$ MLs and (b) with $q = 8$ MLs) makes clear that the smoothing of the transmission profiles is mainly caused by the variations in the Co thickness, independent of the Cu spacer thickness. It is the direct consequence of the corresponding changes in the electronic structure landscape evidenced by the BSFs in figure 3.

Indeed, one might conclude from figures 7(a) and (b) that the Cu spacer only plays the role of a 'propagation medium' of varying size, without too much of an influence on the main features of the transmission profile. Such an interpretation is apparently supported by the results displayed in figure 7(c) for different transmission curves at fixed $m = 8$ MLs and varying Cu thickness q. It is only true, however, for thicker Co layers, in which case the interface-related effects have a smaller weight. In the range of thin Co layers (small m values) the spatial separation of the interfaces within the non-spin-polarized spacer will also affect the transmission profiles, albeit in a more subtle way and on a smaller scale. This can be seen by comparing the two curves labelled $m = 4$ in the two panels (a) and (b) of figure 7.

To summarize, significant changes in the transmission profiles occur when the thickness of the Co layers is varied. We could establish a direct connection between these variations and the modifications in the electronic structure. In turn, a thickness increase of the Cu leads to less spectacular changes in $\mathcal{T}(E)$. Despite the difference in the magnitude of the two effects, we will show, in the next section, that the Seebeck coefficient as well as the MTP are equally sensitive to both m and q variations.

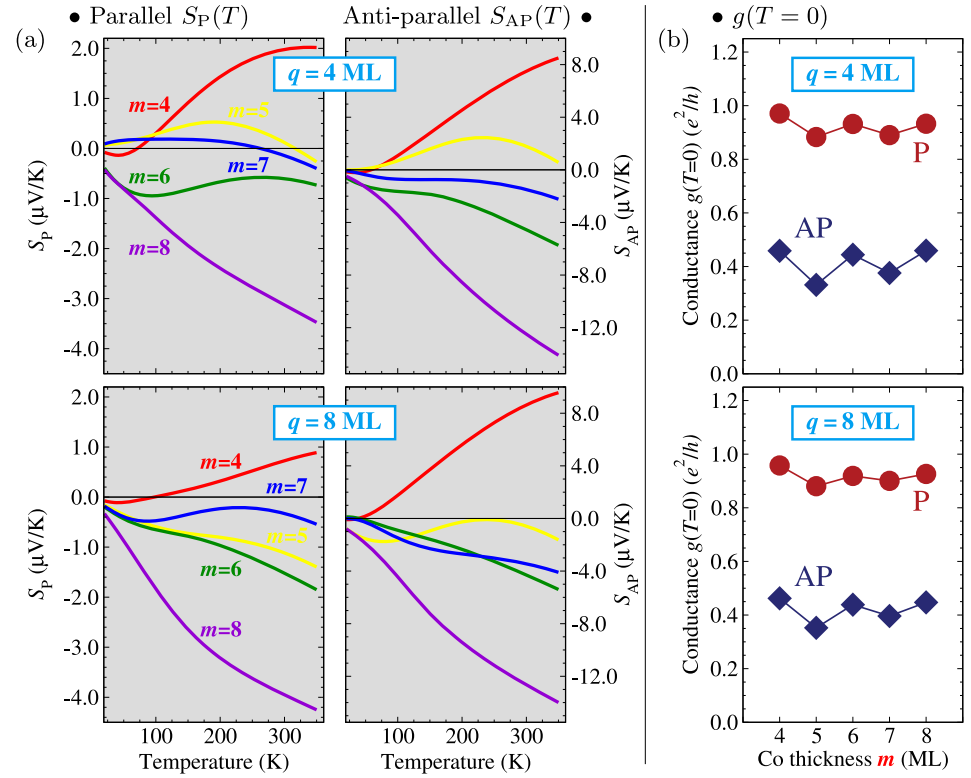

Figure 8. Dependence of (a) the Seebeck coefficient $S(T)$ and (b) the zero temperature conductance $g\,(T=0)$ on the Co layer thickness m (in MLs) in the Cu[3(Co$_m$/Cu$_q$)/Co$_m$]Cu multilayered systems for $q=4$ (top) and $q=8$ MLs (bottom). (a) $S_P\,(T)$ for parallel (P, left panel) and $S_{AP}\,(T)$ for anti-parallel (AP, right panel) alignment of the magnetization in the Co layers. (b) Conductance for P (bullets) and AP (diamonds) alignments. Note that while a different scale is used for $S_P\,(T)$ and $S_{AP}\,(T)$, each of them remains unchanged when varying the Cu thickness q.

5.2. Seebeck coefficient and magneto-thermopower for varying Co thickness

Thermopower measurements on Ni and Fe–Ni films [52] have shown that even at a 20 nm thickness of the sample, the Seebeck coefficient is about half the value measured for bulk. This is a general characteristic of nano-structured metallic systems and the transition from thin films to bulk can be understood as resulting from the reduced weight of the interface-related transmission channels. With an increased thickness of the film, the s- and p-states will have an enhanced contribution to the transmission above the Fermi energy. Specific to the currently investigated systems, both $S_P\,(T)$ and $S_{AP}\,(T)$ turn negative for larger m and q values, with significantly increased absolute values.

This behaviour is illustrated in figure 8(a) where we show the Seebeck coefficients for the parallel (P, left) and anti-parallel (AP, right) magnetic alignments of the Cu[3(Co$_m$/Cu$_q$)/Co$_m$]Cu multilayered system with a fixed Cu spacer thickness $q=4$ MLs (top) and $q=8$ MLs (bottom), for varying Co thickness m. The most spectacular result, anticipated from the changes in the transmission profiles, is the change in sign obtained for both $S_P\,(T)$ and $S_{AP}\,(T)$ when m increases. Note that the same colour-coding convention (from red to purple for increasing m) is used in this figure as introduced above. The m-dependence of $S(T)$ patterns, both in P- and AP-alignment, show remarkable similarities for the two q values, indicating the less important role played by the Cu spacer in governing the (magneto)thermoelectric properties of the investigated systems. Notable differences can only be seen for $m=5$ and $m=7$ MLs Co. In these systems the Seebeck coefficient has a small absolute value and fluctuating sign, as seen, for example in the $S_P\,(T)$ corresponding to $(m,\ q)=(5,\ 4)$ and $(5,\ 8)$.

For the same systems and geometrical parameters we show in figure 8(b) the calculated zero-temperature conductance $g\,(T=0)$. In contrast to the Seebeck coefficient, the conductance is seen to exhibit much less fluctuation with m and q. The reason for this different behaviour lies, once again, in the actual energy range where the transmission probability is changing with m. As we could see, this essentially takes place ±0.2 eV away from the Fermi energy and, as such, does not affect $g\,(T=0)$. Quantum confinement effects do manifest, however, in the conductance: a clear separation in the m-dependence for even and odd values is evidenced in figure 8(b). This originates from the parity dependence of the standing waves formed inside the Co layers by the interaction of the interface states at either side.

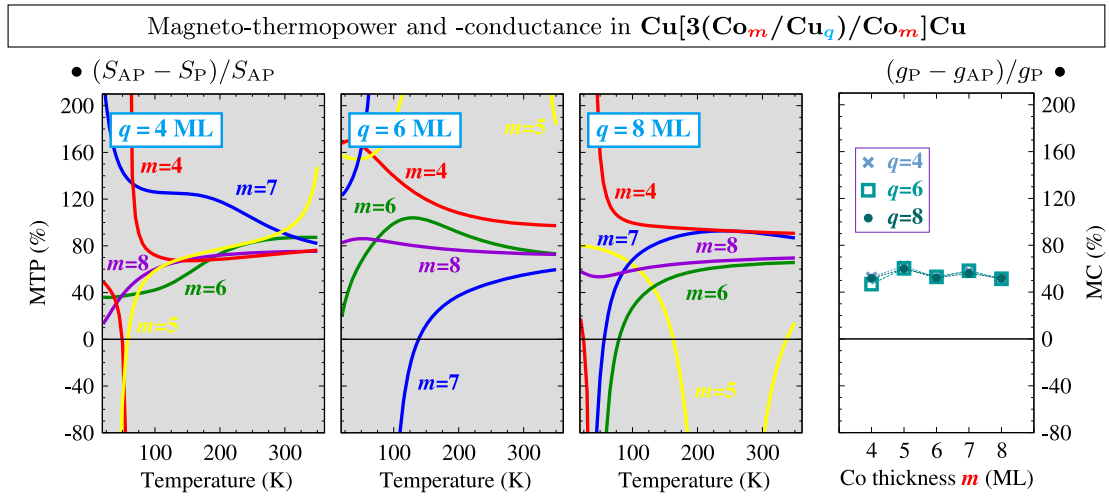

Figure 9. Dependence of the magneto-thermopower (MTP/left) and the zero temperature magneto-conductance (MC/right) on the Co layer thickness m (in MLs) in the Cu[3(Co$_m$/Cu$_4$)/Co$_m$]Cu multilayered systems.

Coming back to the Seebeck coefficient calculated for the two magnetic alignments, P and AP, we note that, regardless of the explicit m and q values, large differences are predicted between $S_{AP}(T)$ and $S_P(T)$. Since, on the other hand, these differences are not independent of T, a rather broad range of values can be expected for the MTP. The temperature-dependent MTP ratios are shown in figure 9 (left panel) for various Cu spacer thickness q and compared with the zero temperature MC (right panel) on an identical scale.

As can be seen in this figure, the range of attained MTP values is much broader than that of the corresponding MC. The latter exhibits slight fluctuations with m, but it remains in an interval of 40–60%, rather independent of the Cu spacer thickness q. Note that, as was the case for the N-varying systems, exceedingly large values of the MTP ratios, caused by $S_P(T)$ approaching zero, are not displayed. For temperatures higher than 100 K, the MTP is obviously larger than the MC, essentially any MTP ratio between 40 and 100% being accessible by an appropriate (m, q) selection.

While this is merely of theoretical interest, as not any (m, q)-combination is necessarily attainable experimentally or energetically stable, the results point to an important aspect. As far as the electronic structure contribution to the transport properties is concerned, using a thermal gradient rather than an electric field could indeed be more advantageous in order to gain a large magnetic sensitivity in a magnetic read-out device.

5.3. Seebeck coefficient and magneto-thermopower for varying Cu thickness

In order to complete our discussion, we analyze how the change on the Cu spacer size, at a fixed Co thickness, influences the transport properties of the Cu[3(Co$_m$/Cu$_q$)/Co$_m$]Cu multilayered systems. As illustrated by the transmission profiles shown in figure 7(c) for fixed $m = 8$ MLs and varying q, the role of the Cu thickness in modelling the transmission is minor: once a basic shape in the energy dependence of the transmission is set by the given Co thickness m, i.e., by filtering and smoothing the QWS-related channels, no significant changes occur in $\mathcal{T}(E)$ as q increases.

This is accordingly reflected in the temperature dependence of the Seebeck coefficient for both P- and AP-alignments shown in figure 10(a). The $S_P(T)$ and $S_{AP}(T)$ curves corresponding to various q values are grouped together over the whole temperature range. The notable exception is the $m = 4$ MLs system in P-alignment, where the formed QWS–p-band complexes couple stronger across the Cu spacer. In contrast, for $m = 4$ MLs in the AP-alignment the $S_{AP}(T)$ values of the different spacer thickness are fairly close to another because the electron scattering is essentially spin-conserving. For the AP magnetic configuration this corresponds to an effective spacer between the Co layers larger than the actual physical one. For a Co thickness $m = 8$ MLs, equivalent to an absence of the QWS–p-band enabled channels, the variations with q of both $S_P(T)$ and $S_{AP}(T)$ is even more reduced. This behaviour is consistent with the experimental findings of Shi *et al* [4] in Co/Cu multilayers of comparable thickness but in a CIP geometry.

The corresponding zero temperature conductance results shown in figure 10(b) follow a similar characteristic of a rather weak dependence on q at a fixed m. We note in particular the complete absence of any oscillations in $g(T = 0)$ between odd and even q, as was the case of varying m.

In spite of the much smaller spread over varying q of both $S_P(T)$ and $S_{AP}(T)$ at fixed $m = 8$ MLs, the MTP ratio still exhibits a broad range of values, as shown in the left panel of figure 11. Above $\simeq$100 K, however, the

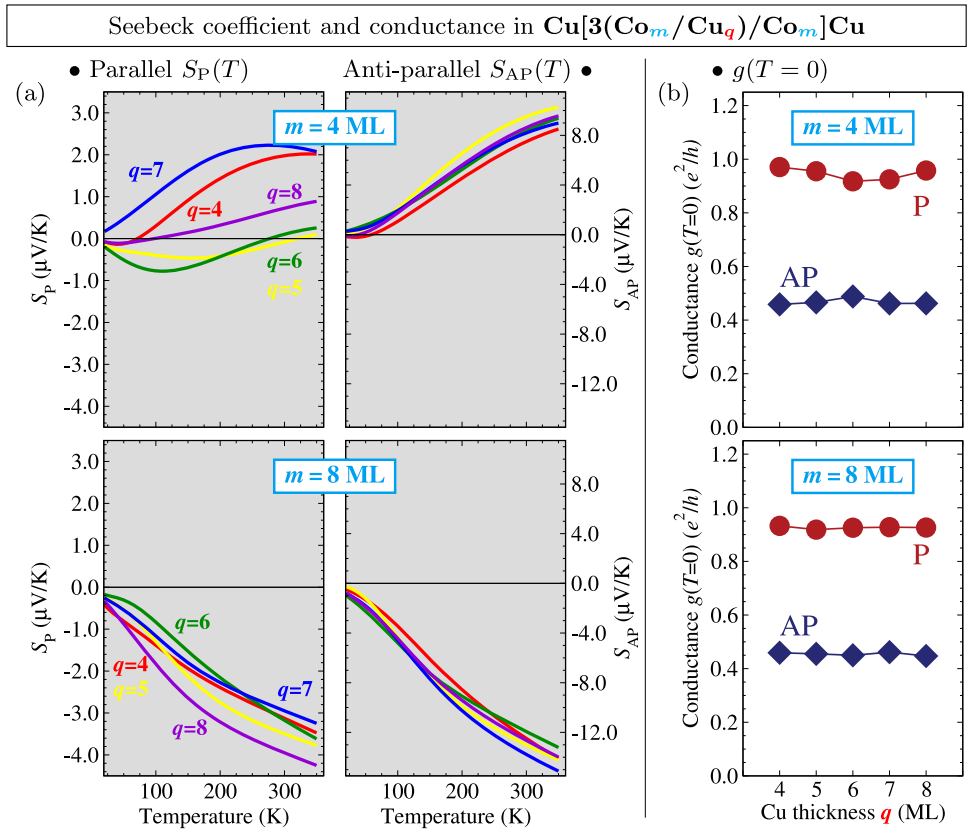

Figure 10. Same as figure 8 but showing the variation of $S_P(T)$, $S_{AP}(T)$, and $g(T=0)$ in Cu[3(Co$_m$/Cu$_q$)/Co$_m$]Cu with the Cu layer thickness q for $m=4$ (top) and $m=8$ (bottom). Note that in panel (a) the same scale is used column-wise, that is, when comparing $S_{P/AP}(T)$ for varying Co thickness m, while the scales are different for $S_P(T)$ and $S_{AP}(T)$ at equal m.

temperature dependence of the MTP for a fixed q is much weaker, even for small values of the Cu spacer thickness. In contrast to the MTP, the MC ratio (right panel) is almost independent of q, showing small fluctuations around 50%. This proves, once again, that the MTP offers in principle a much larger sensitivity to small changes in the electronic structure than the MC. It also implies that the reproducibility of independent experimental data might turn into a problematic issue. In addition, we note that the analysis of the results of this section, encompassing different (m, q) combinations, does not lead to any obvious correlation between the MC and the MTP, nor does it enable us to make definite statements about one configuration being better suited than another for an enhanced MTP.

6. Conclusions

In summary, we have presented results of *ab initio* calculations of the magneto-thermoelectric properties for a series of Co/Cu multilayered systems embedded in Cu(001) with the general formula Cu[$(N-1)$(Co$_m$/Cu$_q$)/Co$_m$]Cu. Our investigations focused on the influence the various morphological parameters—number of repeats N, layer thickness m and q—have upon the underlying electronic structure and, through the induced modifications, on the various transport properties of the heterostructures.

While adopting a spin-polarized fully relativistic formalism, we have nevertheless found that the electronic transmission in the Co/Cu multilayers is to a large extent spin-conserving. For thin Co layers ($m \leqslant 7$ MLs) the minority spin channel, although weaker than the majority spin one, strongly modulates the transmission profile. This modulation is caused by quantum well states present in the Co layer which hybridize with a Co/Cu interface-related p-band, thereby opening very efficient transmission channels. We have shown that the energy position of the such-formed hybrid states, which varies as a function of the Co layer thickness, is accordingly reflected in the transmission profiles. Significant changes with m occur, leading to a large sensitivity of the Seebeck coefficient and the magnetothermopower (MTP) to the thickness of the Co layers. The other geometrical parameters, N and q, have a much smaller influence on the transport properties. We need to emphasize, however, the broad range of values that both the Seebeck coefficient and the MTP may attain in such systems, depending on their morphology, which might cause difficulties when comparing theoretical results

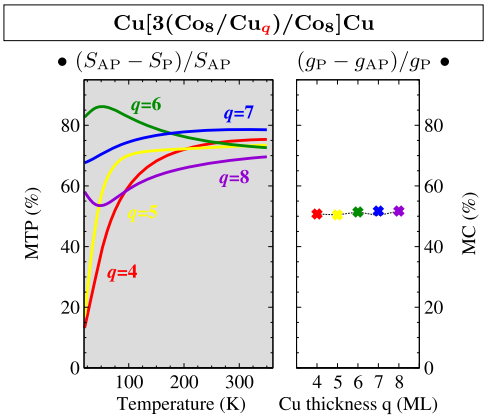

Figure 11. Dependence of the MTP (left panel) and the zero temperature MC (right panel) on the number of Cu layer thickness q in the Cu[3(Co_m/Cu_q)/Co_m]Cu multilayered systems.

with experimental ones. Further effects not considered here, such as thickness fluctuations, interface interdiffusion or relaxation, and defect formation in grown multilayered components, might increase the spread of the results even more.

A comparison of the MTP behaviour to that of the magneto-conductance at the same geometry leads to the conclusion that an MTP read-out of the magnetization state can be equally or even more efficient than a GMR-based device. Our results suggest that a small number of Co layers with precise control of the layer thickness may be more advantageous for this purpose than increasing the number of the Co repeats.

Acknowledgements

This work was supported by the German Research Foundation (*Deutsche Forschungsgemeinschaft — DFG*) within the Priority Program 1538 'Spin Caloric Transport (SpinCaT)'. The authors gratefully acknowledge the computing time granted by the John von Neumann Institute for Computing (NIC) and provided on the supercomputer JUROPA at Jülich Supercomputing Centre (JSC). Additional computer facilities were offered by the Center for Computational Sciences and Simulation (CCSS) at the University Duisburg-Essen.

References

[1] Gijs M A M and Bauer G E W 1997 *Adv. Phys.* **46** 285–445
[2] Conover M J, Brodsky M B, Mattson J E, Sowers C H and Bader S D 1991 *J. Magn. Magn. Mat.* **102** L5–8
[3] Piraux L, Fert A, Schroeder P, Loloee R and Etienne P 1992 *J. Magn. Magn. Mat.* **110** L247–53
[4] Shi J, Yu R C, Parkin S S P and Salamon M B 1993 *J. Appl. Phys.* **73** 5524–6
[5] Nishimura K, Sakurai J, Hasegawa K, Saito Y, Inomata K and Shinjo T 1994 *J. Phys. Soc. Japan* **63** 2685–90
[6] Baily S A, Salamon M B and Oepts W 2000 *J. Appl. Phys.* **87** 4855–7
[7] Scharf B, Matos-Abiague A, Žutić I and Fabian J 2012 *Phys. Rev.* B **85** 085208
[8] Gravier L, Fábián A, Rudolf A, Cachin A, Wegrowe J E and Ansermet J P 2004 *J. Magn. Magn. Mat.* **271** 153–8
[9] Gravier L, Serrano-Guisan S, Reuse F and Ansermet J P 2006 *Phys. Rev.* B **73** 024419
[10] Böhnert T, Vega V, Michel A K, Prida V M and Nielsch K 2013 *Appl. Phys. Lett.* **103** 092407
[11] Böhnert T *et al* 2014 *Phys. Rev.* B **90** 165416
[12] Hu X K, Krzysteczko P, Liebing N, Serrano-Guisan S, Rott K, Reiss G, Kimling J, Böhnert T, Nielsch K and Schumacher H W 2014 *Appl. Phys. Lett.* **104** 092411
[13] Mott N F and Jones H 1958 *The Theory of the Properties of Metals and Alloys* (New York: Dover)
[14] Kudrnovský J, Drchal V, Turek I and Weinberger P 1994 *Phys. Rev.* B **50** 16105–8
[15] Nordström L, Lang P, Zeller R and Dederichs P H 1994 *Phys. Rev.* B **50** 13058–61
[16] Krompiewski S, Süss F and Krey U 1995 *J. Magn. Magn. Mat.* **149** L251–4
[17] Lang P, Nordström L, Wildberger K, Zeller R, Dederichs P H and Hoshino T 1996 *Phys. Rev.* B **53** 9092–107
[18] Butler W H, Zhang X G, Nicholson D M C, Schulthess T C and MacLaren J M 1996 *J. Appl. Phys.* **79** 5282
[19] Weber W, Bischof A, Allenspach R, Würsch C, Back C H and Pescia D 1996 *Phys. Rev. Lett.* **76** 3424–7
[20] Szunyogh L, Újfalussy B, Blaas C, Pustogowa U, Sommers C and Weinberger P 1997 *Phys. Rev.* B **56** 14036
[21] Xia K, Zwierzycki M, Talanana M, Kelly P J and Bauer G E W 2006 *Phys. Rev.* B **73** 064420
[22] Binder J, Zahn P and Mertig I 2000 *J. Appl. Phys.* **87** 5182
[23] Blaas C, Szunyogh L, Weinberger P, Sommers C, Levy P M and Shi J 2002 *Phys. Rev.* B **65** 134427
[24] Sommers C and Weinberger P 2005 *Phys. Rev.* B **72** 054431
[25] Popescu V and Kratzer P 2013 *Phys. Rev.* B **88** 104425
[26] Kováčik R, Mavropoulos P, Wortmann D and Blügel S 2014 *Phys. Rev.* B **89** 134417
[27] Popescu V, Ebert H, Papanikolaou N, Zeller R and Dederichs P H 2004 *J. Phys. Condens. Matter* **16** S5579

[28] Popescu V, Ebert H, Papanikolaou N, Zeller R and Dederichs P H 2005 *Phys. Rev.* B **72** 184427
[29] Ebert H, Ködderitzsch D and Minár J 2011 *Rep. Prog. Phys.* **74** 096501
[30] Bruno P 1993 *J. Magn. Magn. Mat.* **121** 248
[31] Bruno P 1993 *Europhys. Lett.* **23** 615
[32] Krompiewski S, Süss F and Krey U 1994 *Europhys. Lett.* **26** 303
[33] Krompiewski S, Süss F, Zellermann B and Krey U 1995 *J. Magn. Magn. Mat.* **148** 198–9
[34] Ortega J E, Himpsel F J, Mankey G J and Willis R F 1993 *Phys. Rev.* B **47** 1540–52
[35] Ebert H *et al* 2015 The Munich SPR-TB-KKR Package (http://ebert.cup.uni-muenchen.de/spr-tb-kkr.)
[36] Szunyogh L, Újfalussy B, Weinberger P and Kollár J 1994 *Phys. Rev.* B **49** 2721–9
[37] Zeller R, Dederichs P H, Újfalussy B, Szunyogh L and Weinberger P 1995 *Phys. Rev.* B **52** 8807
[38] Wildberger K, Zeller R and Dederichs P H 1997 *Phys. Rev.* B **55** 10074–80
[39] Baranger H U and Stone A D 1989 *Phys. Rev.* B **40** 8169
[40] Mavropoulos P, Papanikolaou N and Dederichs P H 2004 *Phys. Rev.* B **69** 125104
[41] Vosko S H, Wilk L and Nusair M 1980 *Can. J. Phys.* **58** 1200
[42] Turek I, Drchal V, Kudrnovský J, Šob M and Weinberger P 1997 *Electronic Structure of Disordered Alloys Surfaces and Interfaces* (Boston: Kluwer Academic)
[43] Sivan U and Imry Y 1986 *Phys. Rev.* B **33** 551–8
[44] Ködderitzsch D, Chadova K, Minár J and Ebert H 2013 *New J. Phys.* **15** 053009
[45] Wysocki A L, Sabirianov R F, van Schilfgaarde M and Belashchenko K D 2009 *Phys. Rev.* B **80** 224423
[46] Kudrnovský J, Drchal V, Turek I, Khmelevskyi S, Glasbrenner J K and Belashchenko K D 2012 *Phys. Rev.* B **86** 144423
[47] Mahfouzi F and Nikolić B K 2014 *Phys. Rev.* B **90** 045115
[48] Irkhin V Y and Katsnelson M I 2006 *Phys. Rev.* B **73** 104429
[49] Chioncel L, Sakuraba Y, Arrigoni E, Katsnelson M I, Oogane M, Ando Y, Miyazaki T, Burzo E and Lichtenstein A I 2008 *Phys. Rev. Lett.* **100** 086402
[50] Jonson M and Mahan G D 1980 *Phys. Rev.* B **21** 4223–9
[51] Czerner M, Bachmann M and Heiliger C 2011 *Phys. Rev.* B **83** 132405
[52] Avery A D, Pufall M R and Zink B L 2012 *Phys. Rev.* B **86** 184408